Applied Catalysis B: Environmental 198 (2016) 318–324

Contents lists available at ScienceDirect

Applied Catalysis B: Environmental

journal homepage: www.elsevier.com/locate/apcatb

Engendering anion immunity in oxygen consuming cathodes based on Fe-N_x electrocatalysts: Spectroscopic and electrochemical advanced characterizations

U. Tylus[a], Q. Jia[a], H. Hafiz[b], R.J. Allen[a], B. Barbiellini[b], A. Bansil[b], S. Mukerjee[a,*]

[a] Northeastern University Center for Renewable Energy Technology, Department of Chemistry and Chemical Biology, Northeastern University, Boston, MA 02115, USA
[b] Physics Department of Northeastern University, Boston, MA 02115, USA

ARTICLE INFO

Article history:
Received 13 January 2016
Received in revised form 18 May 2016
Accepted 22 May 2016
Available online 27 May 2016

Keywords:
ORR
Non-PGM catalysts
Catalyst poisoning
Chlorine evolution

ABSTRACT

Oxygen reduction reaction (ORR) is the key reaction utilized for several potentially promising technologies such as in energy conversion (fuel-cells) or as oxygen depolarized cathodes (ODC) in anodic evolution of bulk chemicals such as chlorine. In the latter case elimination of one volt out of a theoretical maximum of 1.34 V (in case of hydrogen evolution electrode) provides very significant energy savings. Here we report iron based Fe-N_x catalyst with promising activity compared to state of the art noble metal catalysts (Rh_xS_y) for hydrochloric acid recovery systems. A combined electrochemical and synchrotron-based spectroscopic approach is used to probe the structural and elec tronic properties of the active centers. The surface sensitive delta-mu (Δm) analysis of the near edge X-ray absorption fine structure (NEXAFS), supported by first-principles calculations, reveals the immunity of the Fe-N_x-C_y active centers to chloride poisoning. Initial stability studies show that even after a harsh corrosive treatment, the catalyst ORR activity remains comparable to the current state of the art precious based material. Our study opens up promising avenues for developing affordable and robust oxygen consuming electrodes.

1. Introduction

Catalyst poisoning is a widely recognized problem in elec trocatalysis that inhibits catalytic activity resulting from both specific adsorption (i.e. chemisorption) of anionic species [1–4] (especially in aqueous acidic pH) and non-specific interactions [5] such as passivation via degradation of the electrolyte or other species at the interface. Such poisoning issues, especially specific adsorption, are particularly germane in the case of supported noble metal catalysts (e.g. Pt, Rh, Ru) resulting in increase of overpotential [4–7], and its side effects such as corrosion and eventual metal dissolution. This specific adsorption of specifically halide ions such as chloride and bromide [8] is mainly initiated at positive potentials with respect to the potential of zero charge, which is a factor relevant to the onset and preservation of the ORR.

A cure for this poisoning involves the use of ODC electrodes for bulk production of chemicals such as chlorine, a vital chemical for waste water treatment and other chemical and pharmaceutical applications [9]. Two major processes for chlorine production are electrolytic conversion of brine solution (chlor-alkali cells) [10] and recycling of hydrochloric acid [11,12] where major progress has been made through the use of ODC electrodes in membrane cells in lieu of hydrogen evolving cathodes [13]. This results in saving 1 V (room temperature theoretical potential of ORR being 1.23 V and that of chlorine evolution, 1.36 V vs. RHE), which constitutes major energy savings amounting to an average of ~700 kWh per ton of Cl_2 (g) [14]. This figure is particularly impressive if we consider that currently 2% of total energy consumption in USA is used for chlorine production [9]. Despite the use of noble metals (typically Ag for chlor-alkali and the more expensive Rh_xS_y for HCl recovery), there is a severe inhibition of ORR activity as a result of halide poisoning. Unlike the alkaline pH of the chlor-alkali process, HCl recovery process is especially challenging due to the presence of a harsh chlorine saturated acidic environment in which transition beyond the potential of zero charge results in immediate poisoning by anions [15], even at very low concentrations [8]. Moreover, as chloride ions are carried from the anode through the ion conducting membrane during normal cell operation or during cathode flooding in an uncontrolled power shutdown, the Cl^- concentration on the cathode can rise to 1–5 molar. At these concentrations platinum is known to dissolve [15]. The only catalyst known to withstand the corrosive and poisonous presence of chloride anions is rhodium sul-

* Corresponding author.
E-mail address: s.mukerjee@neu.edu (S. Mukerjee).

http://dx.doi.org/10.1016/j.apcatb.2016.05.054
0926-3373/

fide (Rh_xS_y) [11,16]. Rh_xS_y, although stable (extremely expensive but successfully commercialized [15,17]) in a chlorine saturated chloride environment, is still susceptible to poisoning with a high overvoltage for ORR albeit lower than supported Pt electrocatalysts [16]. This is particularly relevant because, in contrast to supported Pt and Pt alloy nano-particles, Rh_xS_y is a composite of three crystalline phases [18], and hence it does not present a contiguous metal surface as is the case with a supported nano-particle (Pt/C for e.g.,). Promoting ORR in a halide ion containing acidic pH requires the use of very selective sites, which would be immune to anion adsorption. Multi-phasic Rh_xS_y is one such case where the Rh_3S_4 phase provides the active sites for ORR [18]. A logical extension of this argument points toward Heme type moieties, which are one of the most selective sites in this context. Recently, significant advances in ORR electrocatalyst activity have been reported with such bio-inspired active sites [19–22] hereto referred to as metal N-C systems. In contrast to decades of prior efforts [23–25] wherein organic macrocycles containing metallo-Heme type centers (e.g. phthalocyanines or porphyrins) were pyrolyzed on electronically conducting supports such as carbon black, a significant improvement in activity has been achieved more recently with formation of metal-N coordinated sites using non Heme containing simple precursor materials. One early rendition, which we have referred to as the 'reactive polymer approach', involved the use of poly(vinyl amine guanidine) [26].

In this work, we explore the behavior of an ODC cathode electrode containing Fe-N type active sites in operation in the harsh chlorine saturated HCl environment typical of the HCl recovery process. We delineate the efficiency of such Fe-N_x based site, which remains stable and active in a harsh environment where even Pt dissolves. We present a comprehensive investigation of the immunity towards halide ion adsorption using a combination of in situ synchrotron x-ray absorption spectroscopy (XAS), electrochemistry, and density functional theory (DFT) based first-principles calculations.

2. Materials and methods

All experiments reported in this study were carried out on Fe-N_x-C catalysts (poly-FeN_xC) developed in-house by high temperature pyrolysis of a polymer-N/Fe network, using crosslinked and complexed polyethylene imine (xPEI) supported on carbon black (see Supplementary information for details). *In situ* x-ray absorption spectroscopy was employed to identify the various structural and electronic forms of iron centers present in the investigated catalysts. Data collection and analysis of the extended (EXAFS) and near (NEXAFS) XAFS structure, including Delta-Mu ($\Delta\mu$), is described in the Supplementary information. All electrochemical measurements were performed at room temperature using rotating ring-disk electrode (RRDE) equipment purchased from Pine Instruments connected to an Autolab (Ecochemie Inc., model-PGSTAT 30) bipotentiostat. The 1 M $HClO_4$ and 1 M and 5 M HCl electrolytes were prepared from 70% double distilled perchloric acid (GFS Chemicals) and 34% hydrochloric Acid (Alfa Aesar), respectively. A 30% Pt/C catalyst from BASF-ETEK (Somerset, NJ) and 30% Rh_xS_yC from De Nora Tech (Concord, OH) were used as received. Catalyst inks were prepared by ultrasonically dispersing the catalyst powder in a 1:3 (by volume) ratio of water/isopropanol solution. The typical Fe-N_xC catalyst loading employed was 600 $\mu g/cm^2$ (~15–20 $\mu gFe/cm^2$) and 15 $\mu g/cm^2$ of metal in case of Pt/C and Rh_xS_y/C, respectively, on a 0.196 cm^2 glassy carbon disk. Reversible hydrogen electrode (RHE) generated using the same electrolyte as the bulk was used as the reference electrode for the Cl^- dosing study, and Ag/AgCl was used with 1 M HCl as electrolyte. All current values are normalized to the geometric area of the glassy carbon disk unless otherwise stated. All potentials are referred to the RHE scale. Removal of the surface bound iron nanoparticles present in the xBPEI-Fe catalysts was achieved by boiling the catalyst in hot (100C, 2 h) 5 M hydrochloric acid solution saturated with chlorine gas. Procedure this was chosen to simulate a harsh corrosive environment, worst case scenario, which can occur in situation of flooding of the cathode with hot (55–60 °C) concentrated (up to 5 M) HCl and saturated with chlorine evolved during the electrolysis process.

Theoretical calculations were performed using the Vienna Ab initio Simulation Package (VASP) code [27–29] for two different model clusters: FeN_4C_{10} (Fig. 5a) representing Fe-N_4 centers in a perfect graphene plane; and, Fe-N_4-C_8 (Fig. 5b) simulating Fe-N_4 centers within defective pores at the edge of the carbonceous scaffold. A 4×6 graphene supercell containing 26 carbon atoms was generated using a hexagonal graphene unit cell of 2 atoms. The Fe-N_4 cluster was embedded by creating a carbon divacancy [30]. All the outer carbons in the model clusters were passivated with hydrogen atoms [31]. The Fe-N_4-C_8 model was built by the removal of the two next near neighbor carbon atoms of the Fe site, followed by geometry optimization. These simulations create a fragment Fe-N_4-C_8 similar to the model utilized by Kattel et al. [30]. The core electrons were described by the projector augmented wave (PAW) basis [32] using a cutoff energy of 400 eV to describe the valence electrons. For electronic exchange-correlation effects, we used generalized gradient approximation (GGA) within the Perdew–Burke–Ernzerhof (PBE) parametrization [33] GGA functionals are crucially important in order to describe correctly properties of iron [34]. The DFT calculations were performed with full relaxation of ionic positions until two consecutive relaxations reached an energy difference of less than 0.1 meV. The geometry optimization was carried out using a $2 \times 2 \times 1$ Monkhorst-Pack k-space grid [35]. Spin polarization was included in electronic density of states (DOS) and binding energy calculations. DOS was computed using a denser k-point mesh of $8 \times 8 \times 1$ and a smearing parameter $\sigma = 0.1eV$.

3. Results and discussion

3.1. Effect of Cl^- on ORR polarization curves (RDE)

Fig. 1 presents comparative polarization curves (Fig. 1a), including results after mass transport correction (Fig. 1b), of Fe-N_x-C catalyst derived from a cross-linked network of branched polyethyleneimine complexes, hereafter referred to as poly-FeN_xC, with and without the presence of Cl^-, compared with Pt/C (BASF-ETEK, NY) and Rh_xS_y/C (Denora Tech, OH).

The two noble metal catalysts represent current state-of-the-art for oxygen consuming materials in PEM fuel cells and HCl electrolyzers, respectively [11,16,18]. The rotating disk response (I–V curves normalized to disk geometric area) to ORR without the presence of chlorides displays the expected superiority of the Pt/C and Rh_xS_y/C catalysts over the non-noble metal materials. This is expected in the acidic pH with the performance difference falling within 150 mV in half-wave potential, $E_{1/2}$, (see Supplementary information, Table S1) as reported earlier [20,22,26]. However, addition of Cl^- results in drastic increase of the ORR overpotential for both Pt/C and Rh_xS_y/C, the former being negatively affected to a greater degree. On the other hand, the poly-FeN_xC material shows high resistance against poisoning (Figs. 1a–b). A detailed analysis of the RDE data including the Tafel analysis is provided as Supplementary data (Table S1). The poisoning of the supported noble metal electrocatalyst surface (i.e., Pt/C) by halide ions has been previously studied by Arruda et al. [8]; using an *in situ* XAS/$\Delta\mu$ – XANES technique, a 3-fold bonded Cl^- was shown to poison the surface at

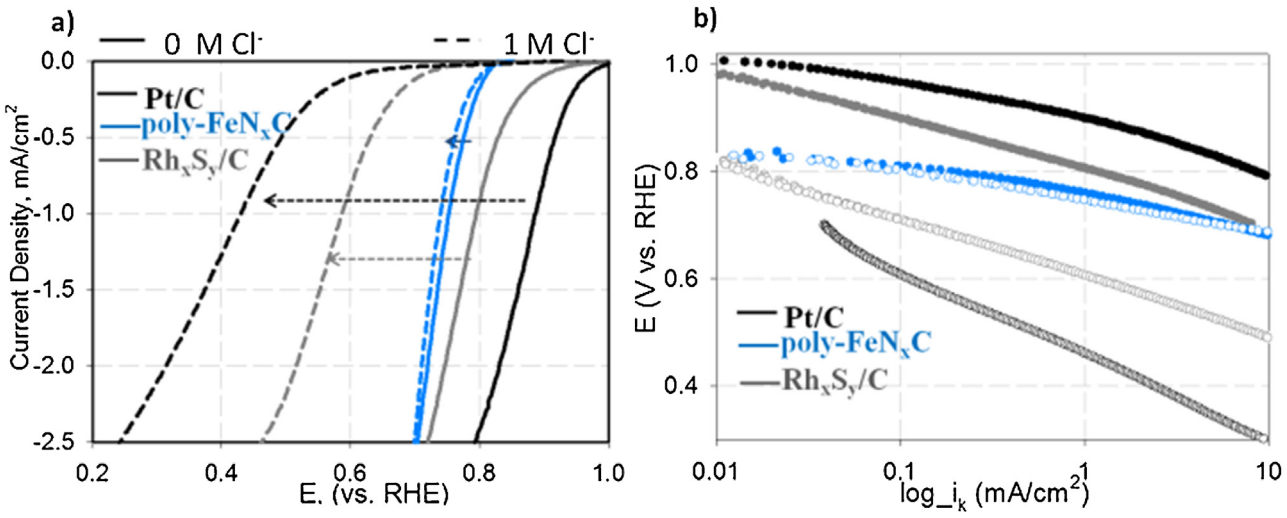

Fig. 1. Comparative ORR polarization curves (a) and the corresponding kinetic current densities (b) of poly-FeN_xC (blue), state of the art rhodium sulfide (grey) and platinum on carbon (black) in 1 M $HClO_4$ (solid lines) and 1 M HCl (dashed lines), RT. RDE @ 20 mV/sec, 900 rpm (GC 0.196 cm^2, Ag/AgCl reference, Carbon cloth counter electrode). (For interpretation of the references to colour in this figure legend, the reader is referred to the web version of this article).

high anion concentration, while a mix of Cl^- and O[H] adsorption was observed at lowerCl^-concentration. Similar systematic studies have not been conducted on Rh_xS_y/C catalysts, although some aspects have been discussed in the literature [11]. Effect of Cl^- for concentration range below 1 M in terms of ORR performance of the three types of the catalysts are shown in Supplementary information (Fig. S1a–f).

3.2. Fe-based active centers

It has been shown that the highest ORR activity of the Fe-N_xC catalysts is related to the presence of two types of metal centers, which have a synergistic effect on the overall catalytic performance: (1) nitrogen coordinated metal sites, Fe-N_x [19,22,36–39] essentially embedded in the microporous frame of the carbon scaffold [22], often labeled as Fe-N_4 [39,25], and, (2) adjacent to the Fe-N moieties metal nanoparticles (NPs) protected by high crystalline carbonaceous platforms [20,40]. The nature of such composite active sites, referred to as Fe-N_xC/Fe_{NPs} moieties, has been reported on [26], demonstrating that the onset potential of ORR on Fe-N_xC catalysts is dictated by the redox potential of the Fe-N_4 center, which is also observed with poly-FeN_xC, the catalyst investigated here (Fig. 2a). Based on our extensive in-situ XAS observations, the onset of ORR is directly related to the activation of the Fe-N_4 site following the transition of Fe^{3+} (oxide form) to Fe^{2+} (*sans* the oxide and adsorption of molecular oxygen) during the cathodic sweep from the rest potential. This redox transition and the coexisting formation of adsorbates (previously verified with a surface sensitive x-ray absorption analysis [26]) may vary depending on the catalyst synthesis method employed. Moreover, properties such as the Lewis basicity of carbon [41], impact the density and electronic properties of the Fe-N_x sites, and therefore govern the overpotentials of the ORR process [41].

3.3. Fe-N_x sites in presence of Cl^-

In the present work, we investigate interaction of Fe-N_x sites with chloride anions in order to understand the viability of this catalyst group for oxygen- depolarized cathodes. Differential XANES technique ($\Delta\mu$-XANES) was used to determine and model the surface-active species of the metal and to identify interactions of those species with the Cl^- against the native oxygenated adsorbates. For theoretical support, DFT calculations were performed to compare binding energies (E_b) between the Fe centers (in Fe-N_x sites) and Cl^- against $^*OH$, and $^*O$. The latter can exist due to the presence of reversible conversion of water to hydroxyl anion ($H_2O \rightarrow OH^- + H^+$) and subsequent formation of oxygen anion ($OH^- \rightarrow O^{2-} + H^+$) [42,43]. The use of $^*OH$, and $^*O$ in the DFT calculations was performed following arguments previously adopted by Rovira and Parrinnello [44] while performing dynamics simulations of models for active centers of myoglobin. As typical to the majority Fe-N_x-C type catalysts, which were discussed in our earlier work [26], majority of the iron species present in the poly-FeN_xC constitute the Fe-N_x moieties with minor contribution from non-coordinated Fe forms, Fe_{NPs}/C (Fig. 2b). While the detailed structure/s of the Fe-N_x centers is/are yet to be understood, an examination of the experimental $\Delta\mu$ – XANES signals against models (Supplementary information, Figs. S3 and S4) suggests ~80–90% contribution from Fe-N_x sites (Fe-N_x-C_8, and/or Fe-N_x-C_{10}, discussed below), while the remaining signal is believed to originate from Fe-O[H] interaction of the non-N_x coordinated Fe.

The introduction of chloride anions causes noticeable suppression of the negative amplitude in the experimental $\Delta\mu$-XANES signatures (Fig. 3a) and this trend becomes more pronounced as the positive potential bias exceeds 0.5 V, reaching the maximum effect at 0.9 V (Figs. 3a–b). This is consistent with a small negative shift of the ORR polarization curve in the presence of chloride anions shown in Fig. 3c. A detailed examination of the experimental $\Delta\mu$-XANES shapes and correlation with the theoretical $\Delta\mu$ profiles (Fig. 3d) suggests that these small changes in ORR activity originate from the Fe-Cl interaction involving only the non-coordinated Fe, no evidence of Cl^- adsorption on the Fe-N_x centers is indicated. This is supported by the fact that theoretical $\Delta\mu$ signature of the Fe-N_x in conjunction with several possible modes of chloride adsorption, differs drastically from the $\Delta\mu$ signal observed experimentally (See Supporting Information, Fig. S6). The observed experimental $\Delta\mu$ signal as a function of potential in the presence of chloride anions remaining close to those observed in its absence. In fact, the minor effect of the chlorides diminishes upon removal of the surface-active nanoparticles (Figs. 4a, b).

The removal of the non-coordinated Fe moieties was achieved via exposure the electrocatalyst to later explained treatment in chlorine saturated concentrated hydrochloric acid. The increase of the amplitude of the EXAFS representing Fe-N interactions are directly proportional to concomitant increase of its relative

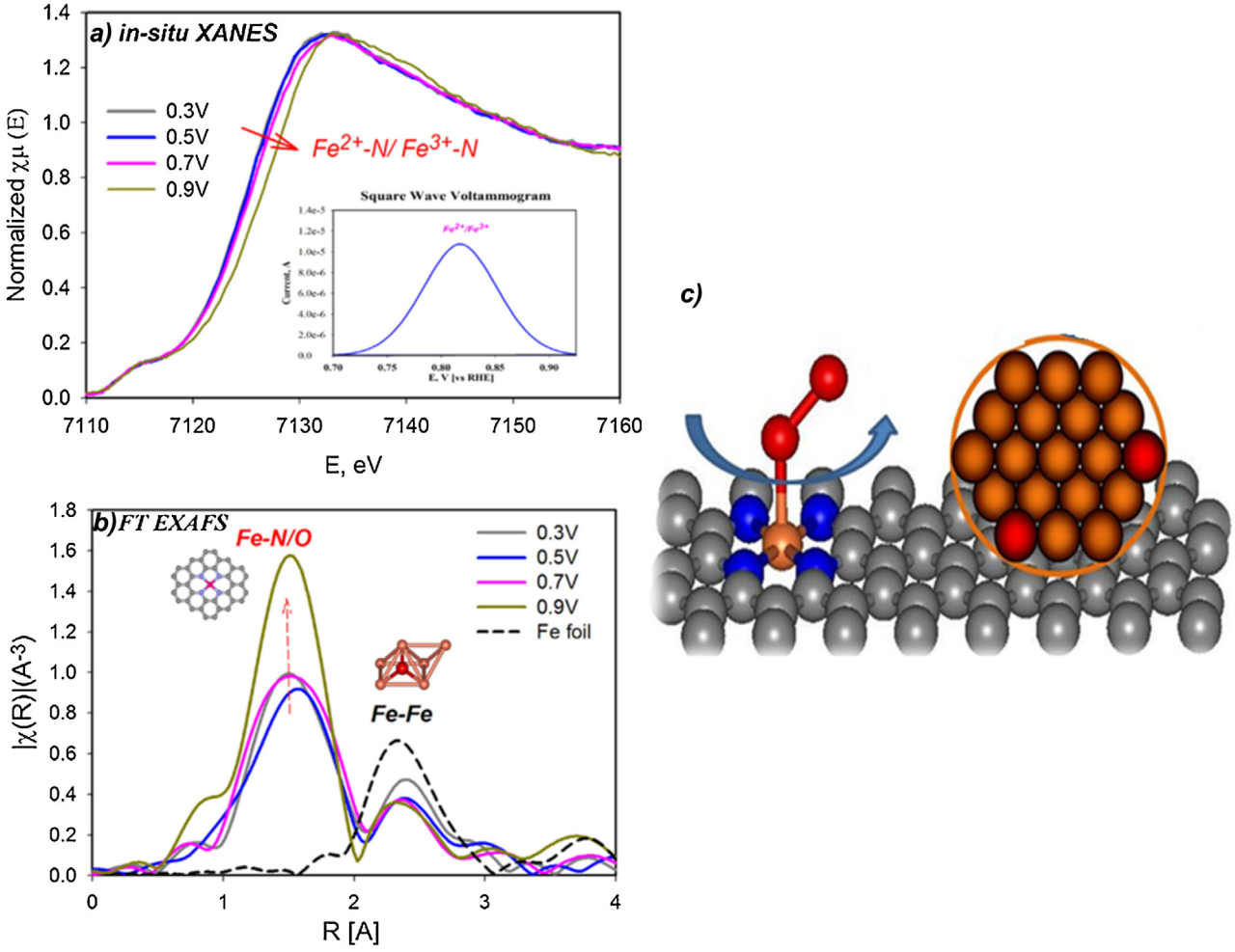

Fig. 2. (a) Potential dependent normalized XANES with related redox peak shown as square wave voltammetry in the inset collected in oxygen-free 0.1 M $HClO_4$, and (b) corresponding Fourier Transforms of EXAFS of the polyFeN_xC (blue) catalyst collected in-situ on Fe k-edge in 0.1 M $HClO_4$, together with that of an iron reference foil (black). The main peak around 1.5 Å represents Fe-N_x form of the metal. The low intensity peaks around 2.2 Å represents Fe–Fe scattering indicating the presence of Fe-nanoparticles in the heat-treated catalyst. c) Schematics representing two forms of iron, Fe-N_x and Fe_{NPs}, detected in the poly-FeN_xC catalyst. *Note: all radial distances given are without phase correction.* (For interpretation of the references to colour in this figure legend, the reader is referred to the web version of this article.)

contribution to the overall coordination number (Fe-N + Fe-Fe). Hence selective removal of uncoordinated Fe species as a result of potential cycling in peroxide containing electrolyte represents the resulting higher contribution from the Fe-N relative to Fe–Fe interactions in the cycled samples. This is shown as a comparison of in situ EXAFS (Fig. 4 (a)) before and after cycling in peroxide laced electrolytes. The comparison of the $\Delta\mu$ obtained by subtraction of 0.8–0.3 V data with and without 100 mM Cl^- shows negligible change post peroxide cycling thereby indicating that the bulk of the contribution to $\Delta\mu$ as a result of exposure to CL^- is due to uncoordinated Fe species (Fig. 4 (b)).

$$\Delta\mu_{observed} = \frac{Fe_{Fe-N}}{Fe_{total}}\Delta\mu_{Fe-N}$$

where,

$Fe_{Fe\text{-}N}$ – Fe atoms contributing to the $\Delta\mu$ signal

Fe_{total} – total Fe atoms detected by XAS

$\Delta\mu_{observed}$ – observed amplitude of the signal

$\Delta\mu_{Fe\text{-}N\text{–}amplitude}$ of $\Delta\mu$ assigned to $Fe_{Fe\text{-}N}$

Furthermore, comparisons of the DFT calculated binding energy E_b at the Fe-N_x center between the ORR intermediates and the chloride ion support our experimental observations. The DFT calculations were performed using the VASP [27–29] code. The same calculations performed with Gaussian method (not shown in the article) yielded the same ground state structure. The DFT conducted here disregards the solvation and entropic effects but is sufficient for comparing the binding energy between the metal and various adsorbates as shown by different research groups [30,43,45]. Three models of the Fe-N_x were used. The Fe-N_4-C_{12} (D2) fragment shown in Fig. 5a is a good representation the Fe-N_x center in an original macrocycle. Similar structures have previously demonstrated immunity to strongly poisoning species such as Cl^- and CO [46,47]. The Fe-N_4-C_{10} (D1) cluster simulates Fe-N_4 center embedded in a graphene plane (Fig. 5b) and the Fe-N_x-C_8 cluster with x = 4 (D1), and 5 (D3) (Fig. 5c and d, respectively) simulates the Fe-N_x centers situated within porous defects and/or at the edge of the carbonaceous platform. The Fe-N_4-C_8 density of states presented in the Supplementary information (Fig. S7a–d) and the Fe-N_4-C_8-OH binding energy were compared with the earlier results by Kattel et al. [30] in order to verify robustness of our VASP calculations. H passivation was used for extracting robust and accurate information [31]. Experimental [48,49] and theoretical [45] studies have discussed the significance of an additional (fifth) ligand/coordinate in the active form of the Fe-N_x center. Such a fragment (shown in Fig. 5d) is also assigned to the important doublet D3, which presents optimal catalytic ORR activity [48]. Effects of the 5th ligand, here denoted as N_{axi} to indicate its axial position to the plane of the Fe center, were considered by computing the binding strengths

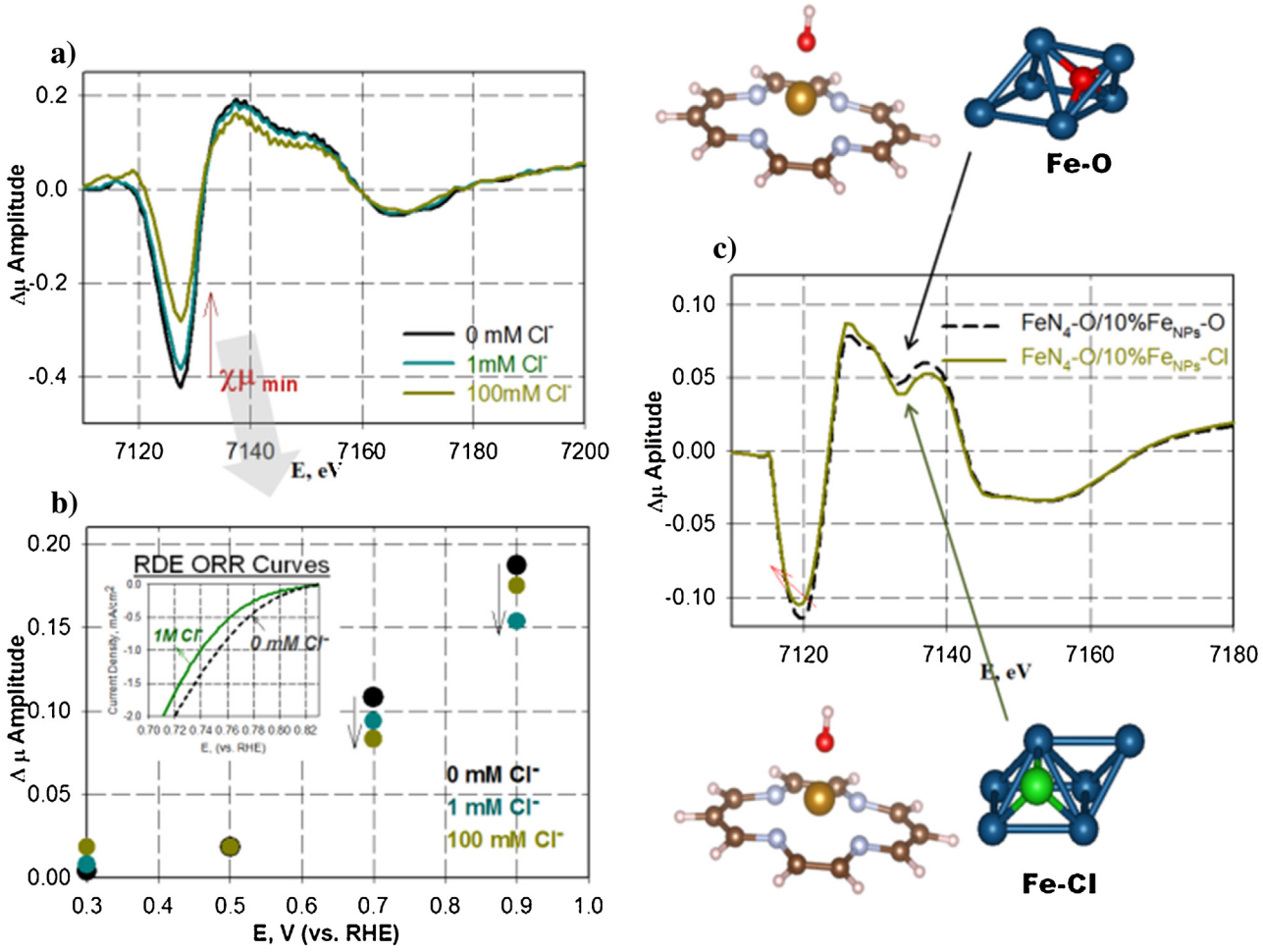

Fig. 3. $\Delta\mu$ spectra of poly-FeN_xC collected in-situ on Fe k-edge as a function of Cl^- concentration at 0.9 V (vs. RHE) (a) and the corresponding $\Delta\mu$ negative peak amplitude plotted as function of potentials (b); the inset in (b) represents ORR polarization curves of the polyFeNC with (as 1 M HCl) and without (in 1 M $HClO_4$) presence of Cl^-. (c) shows theoretical model consisting of 90% FeN_4C_{10}-O and 10% O-Fe_{NPs} (assuming full coverage of the active surface) compared to a theoretical model when the Fe_{NPs}-O interaction is replaced with Fe_{NPs}-Cl. Experimental $\Delta\mu$ signatures were obtained by subtracting the XANES signatures as: $\Delta\mu = \mu(0.90\,V) - \mu(0.30\,V)$. Details of methodology used to obtain the theoretical model, which fits the best to the experimental signatures, is given in Supplementary information (Figs. S3–5).

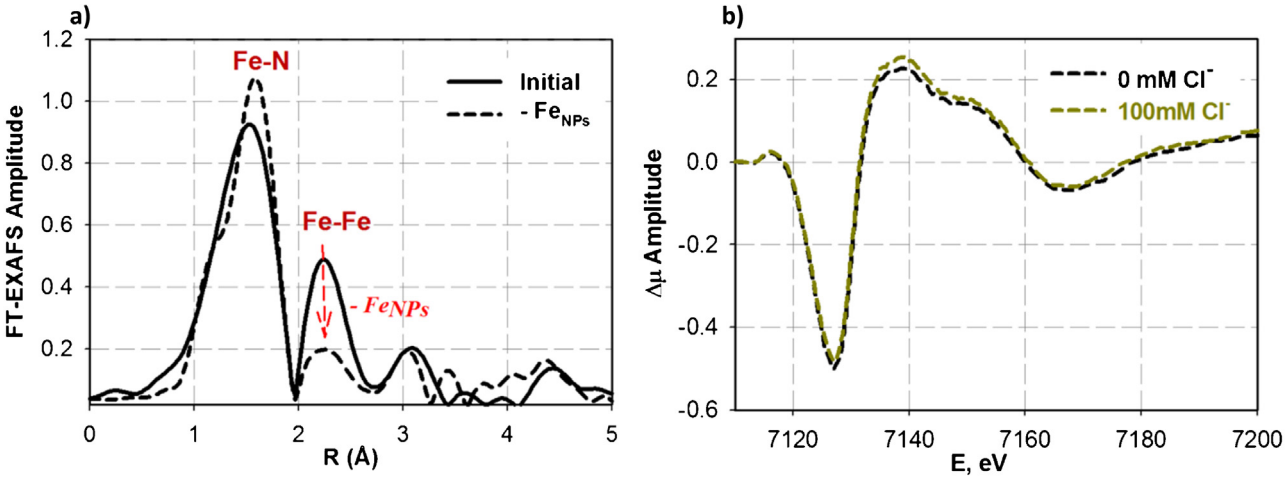

Fig. 4. Fourier Transform of EXAFS spectra on Fe K-edge of the poly-FeN_xC catalysts collected in-situ at 0.3 V before (solid like) and after (dashed line) the removal of the nanoparticles (a), and experimental $\Delta\mu = \mu(0.80\,V) - \mu(0.30\,V)$ of the Fe K-edge XANES spectra collected in-situ in 0.1 M $HClO_4$, after removal nanoparticles in presence of 0 mM Cl^- (black) and 100 mM Cl^-(green) showing no effect of chlorides (b). Note: Effect of NPs removal on $\Delta\mu$ shape against the theoretical signatures is shown in the Supplementary information, Fig. S4). (For interpretation of the references to colour in this figure legend, the reader is referred to the web version of this article.)

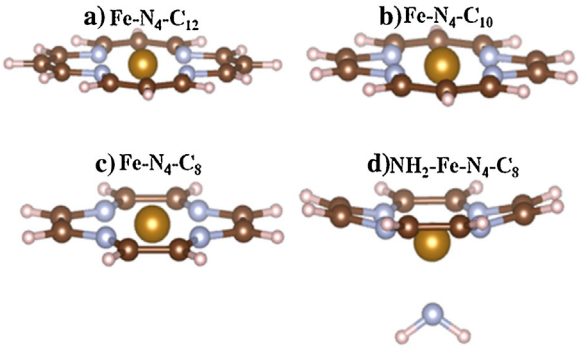

	label	O*	OH*	Cl⁻
Fe-N_4-C_{10}	D1	-4.518	-2.257	-3.000
Fe-N_4-C_8	D1	-5.266	-3.511	-3.810
NH_2-Fe-N_4-C_8	D3	-3.279	-2.606	-2.490
Fe-N_4-C_{12}	D2	-2.897	-3.164	-1.831

Fig. 5. Atomic structures of Fe-N_x centers in the model clusters used for the calculations shown in Table which represent computed binding energies (E_b) in the state of the lowest energy for Fe-N_4-C_{10} (D1), Fe-N_4-C_8 (D1), NH_2-Fe-N_4-C_8 (D3) and Fe-N_4C_{12} (D2). Where, the models represent Fe-N_4 enters (a) in the original macrocycle Fe-N_4-C_{12}, (b) within the defects of graphene plane Fe-N_4-C_{10}, (c) on the graphene edge, Fe-N_4-C_8, and (d) Fe-N_4-C_8 with the additional axial ligand NH_2-Fe-N_4-C_8. In both cases, the carbon atoms were passivated with hydrogen atoms as needed for the DFT calculations.

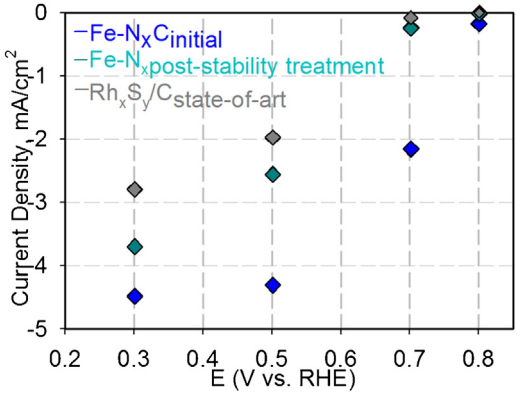

Fig. 6. Potential dependent current densities collected chronoamperometrically in 1 M HCl (room temperature). The poly-FeN_xC @ 0.6 mg_{FeNxC}/cm^2 at initial state (dark blue) and after the treatment (cyan), compared to industrial state-of-the-art Rh_xS_yC @ 1 mg_{Rh}/cm^2 (grey). (RT RDE @ 20 mV/sec, 900 rpm (GC 0.196 cm^2, Ag/AgCl reference, Carbon cloth counter electrode). (For interpretation of the references to colour in this figure legend, the reader is referred to the web version of this article.)

between the NH_2-Fe_4-C_8 and *O(H), Cl^-. The computed results in Table 1 confirm the previously suggested resistance [46,47] of the macrocycle D2 to the poison, which is represented by the differences in the lower E_b value between the Fe-N_4-C_{12} and *OH versus E_b of Cl-Fe-N_4-C_{12}.

A similar trend is seen with Fe-N_4-C_{10}, Fe-N_4-C_8 and N_{axi}-Fe-N_4-C_8. Here, however, the strongest theoretical binding is obtained between the Fe center and the *O exceeding E_b of Fe-*OH. Taking the experimentally observed immunity of the poly-FeN_xC catalyst to the Cl^- into account, the latter computed results suggest preferential formation of Fe-O over the Fe-OH as a result of $H_2O \rightarrow OH^- + H^+$ followed by $OH^- \rightarrow O^{2-} + H^+$ process of water activation. It is well known that the E_b between chlorides and platinum based catalysts significantly exceeds the values of the ORR reactants as the Pt surface is very sensitive to the halides (especially in acid environment), which results in impeded activity of the Pt-based catalysts [8]. The stronger binding strength of the oxygenated species [30,50] with the Fe-N_xC_y compared to the Fe-N_xC_y-Cl binding may be considered as the smoking gun for immunity of the Fe-N_xC based catalysts to chloride poisoning.

3.4. Viability of Fe-N_x-C_y in ODC cathode

Our XAS studies show that such harsh treatment of the Fe-N_x-C catalyst result in removal of the nanoparticles, however, leaving majority of the immune to Cl^- N-coordinated iron centers intact. This exposure of the catalyst to chlorine saturated hot concentrated hydrochloric acid simulates environment, in the ODC cell, to which ORR catalyst is exposed in case of the earlier mentioned uncontrolled shut-down. Considering the Fe-N_x moieties as primary catalytic centers, the shown here properties create a paradigm shift for technologies based on fuel cell applications including ODC in chlorine recycling and recovery. Fig. 6 shows compared to industry standard Rh_xS_y/C (Denora, North America), chronoamperometrically (CA, where the current densities were measured at constant potentials) measured ORR performance of the Fe-N_x catalyst at initial state and after the above treatment. Similarly to the earlier discussed RDE experiments, the CA (10 min hold at each potential) measurements were performed in 1 molar HCl to simulate maximal Cl^- concentration at the cathode of industrially used ODC cell during standard process of electrolytic recovery of chlorine from concentrated HCl, a side-product of various industrial processes, where Cl_2 is used as a reagent (i.e., PVC production). As shown in Fig. 6, exposure of the Fe-N_x based catalysts to such extreme conditions, resulted in partial losses of its catalytic performance, still slightly exceeding ORR activity of the current state-of-the-art Rh_xS_y/C.

To our knowledge, this represents the first report of a Fe-N_x-C catalyst which after exposure to the chlorine saturated HCl environment exhibits performance near to the industry, based noble metal, standard. The current densities of the Fe-N_x after the harsh treatment which are observed to be higher at lower potentials in comparison to the current densities of Rh-catalyst, suggests possibility for even some superiority of the non-noble metal catalyst performance, which could be exploited in case of running the ODC electrolysis process in higher ORR overpotentials. Considering the fact that such non-PGM catalysts have 10^3 times lower active site density [41] compared to the conventional noble metal on carbon catalyst such as Rh_xS_y/C and thereby requiring a thicker electrode structure, we expect that after relevant optimization the Fe-N_x consisting ODC electrodes a 10–20% further energy savings is possible. This saving would add to the significantly lower cost of the catalyst containing Fe when compared to the more expensive Rh. Clearly, these results point to very attractive possibilities for various industrial electrochemical processes, where the noble-metal-free catalysts are suitable as oxygen depolarized cathodes.

4. Conclusions

We have investigated the viability of Fe-N_x containing catalysts as oxygen depolarized cathodes in a chlorine saturated HCl environment, and demonstrated their relative immunity toward ORR activity in the presence of chloride anions. Our electroanalyti-

cal results, supported by carefully designed in-situ spectroscopic experiments, clearly establish the insensitivity of the Fe-N_xC_y centers to Cl^-. Our experimental findings are also supported by corresponding first-principles DFT calculations, which reveal a significantly weaker binding of Cl^- than the native oxygenated species. The resistance to chlorides originates mainly from the nature of the metal-based surface-active functionalities characterizing the Fe-N_x-C_y sites. When the Fe centers are incorporated into the π – electron-deficient graphitic carbon environment, with the carbon being part of the active surface, the electronic structure of Fe undergoes a substantial modification. The behavior of Fe-N_x-C_y centers in thus in sharp contrast to that of the carbon supported ORR active metal nanoparticles, where carbon acts only as a conductive support that anchors the sites. Considering the large body of literature focused on the Fe-N_x-C group catalysts, the presence of different Fe-N_x species within the same material, represented here by the doublets D1 and D3, is very likely. This is also true for the resistance to Cl^- poison exhibited by material studied here. An important result of our study is that all the Fe-N_x-C_y centers are resistant to the detrimental effects of chloride anions. This property suggests novel applications for depolarized cathodes in wide-ranging industrial processes, including the energy efficient electrochemical evolution of chlorine, where the immunity to Cl^- is more important than the superior activity of a catalyst.

Acknowledgements

The authors deeply appreciate financial assistance from the U. S. Department of Energy, EERE (DE-EE-0000459) under which the catalyst materials were made. Tests for the poly-FeN_xC catalyst evaluation for ODC applications were sponsored under a catalyst award provided by the Massachusetts Clean Energy Council (Mass-CEC) and sponsorship by Denora (North America). Use of the National Synchrotron Light Source (NSLS), Brookhaven National Laboratory (BNL), was supported by the U.S. Department of Energy, Office of Basic Energy Sciences. Synchrotron spectroscopy data used in this publication was made possible by the Center for Synchrotron Biosciences grant, P30-EB-009998, from the National Institute of Biomedical Imaging and Bioengineering (NBIB). Support from beamline personnel Dr. Erik Farquhar and Mark Chance (X3B) are gratefully acknowledged.

This work was also supported by the U. S. Department of Energy, Office of Science, Basic Energy Sciences grant number DE-FG02-07ER46352 (core research), and benefited from Northeastern University's Advanced Scientific Computation Center (ASCC), the NERSC supercomputing center through DOE grant number DE-AC02-05CH11231, and support (applications to layered materials) from the DOE EFRC: Center from the Computational Design for Functional Layered Materials (CCDM) under grant number DE-SC0012575.

The authors greatly acknowledge Dr. Kattel Shyam and Dr. Guofeng Wang at University of Pittsburgh for advice on the Fe-N-C models for DFT calculations.

Dr. Andrea Gulla at Denora Tech (Concord, OH) is gratefully acknowledged for providing advice in designing experiments representing environment relevant to industrial HCl electrolysis in ODC cell.

Appendix A. Supplementary data

Supplementary data associated with this article can be found, in the online version, at http://dx.doi.org/10.1016/j.apcatb.2016.05.054.

References

[1] B.E. Conway, Solid State Ionics 94 (1997) 165–170.
[2] A.P. dos Santos, A. Diehl, Y. Levin, Langmuir 26 (2010) 10778–10783.
[3] Y. Levin, Phys. Rev. Lett 102 (2009) 147803.
[4] S. Trasatti, R. Parsons, J. Electroanal. Chem. Interfacial 205 (1986) 359–376.
[5] R. Borup, J. Meyers, B. Pivovar, Y.S. Kim, R. Mukundan, N. Garland, D. Myers, M. Wilson, F. Garzon, D. Wood, Chem. Rev. 107 (2007) 3904–3951.
[6] T.J. Schmidt, U.A. Paulus, H.A. Gasteiger, R.J. Behm, J. Electroanal. Chem. 508 (2001) 41–47.
[7] N. Marković, H. Gasteiger, B. Grgur, P. Ross, J. Electroanal. Chem. 467 (1999) 157–163.
[8] T.M. Arruda, B. Shyam, J.M. Ziegelbauer, S. Mukerjee, D.E. Ramaker, J. Phys. Chem. C 112 (2008) 18087–18097.
[9] A. w. C. Council, Global Voice for the Chlorine http://www.worldchlorine.org.
[10] Y. Kiros, M. Bursell, Int. J. Electrochem. Sci. 3 (2008) 444–451.
[11] J.M. Ziegelbauer, A.F. Gullá, C. O'Laoire, C. Urgeghe, R.J. Allen, S. Mukerjee, Electrochim. Acta 52 (2007) 6282–6294.
[12] J. Perez-Ramirez, C. Mondelli, T. Schmidt, O.F.K. Schluter, A. Wolf, L. Mleczko, T. Dreier, Energy Environ. Sci. 4 (2011) 4786–4799.
[13] I. Moussallem, J. Jörissen, U. Kunz, S. Pinnow, T. Turek, J. Appl. Electrochem. 38 (2008) 1177–1194.
[14] J. Chlistunoff, Advanced chlor-alkali technology, Final Technical Report, LAUR 05-2444. Los Alamos, NM, USA, (2005).
[15] USA Pat., 6, 149, 782, (2000).
[16] A.F. Gullá, L. Gancs, R.J. Allen, S. Mukerjee, Appl. Catal. A: General 326 (2007) 227–235.
[17] R.J. Allen, A.F. Gulla, Google Patents, (2011).
[18] J.M. Ziegelbauer, D. Gatewood, A.F. Gullá, M.J.F. Guinel, F. Ernst, D.E. Ramaker, S. Mukerjee, J. Phys. Chem. C 113 (2009) 6955–6968.
[19] A. Serov, K. Artyushkova, P. Atanassov, Adv. Energy Mater. (2014), http://dx.doi.org/10.1002/aenm.201301735, n/a-n/a.
[20] G. Wu, K.L. More, C.M. Johnston, P. Zelenay, Science 332 (2011) 443–447.
[21] E. Proietti, F. Jaouen, M. Lefèvre, N. Larouche, J. Tian, J. Herranz, J.-P. Dodelet, Nat. Commun. 2 (2011) 416.
[22] M. Lefevre, E. Proietti, F. Jaouen, J.P. Dodelet, Science 324 (2009) 71–74.
[23] R. Jasinski, (1964).
[24] V. Bagotzky, M. Tarasevich, K. Radyushkina, O. Levina, S. Andrusyova, J. Power Sources 2 (1978) 233–240.
[25] J.-P. Dodelet, in: J.H. Zagal, F. Bedioui, J.-P. Dodelet (Eds.), N4-Macrocyclic Metal Complexes, Springer, 2006, 2016, pp. 83–139.
[26] U. Tylus, Q. Jia, K. Strickland, N. Ramaswamy, A. Serov, P.B. Atanassov, S. Mukerjee, J. Phys. Chem. C (2014).
[27] G. Kresse, J. Furthmüller, Phys. Rev. B 54 (1996) 11169–11186.
[28] G. Kresse, J. Hafner, Phys. Rev. B 47 (1993) 558–561.
[29] G. Kresse, D. Joubert, Phys. Rev. B 59 (1999) 1758–1775.
[30] S. Kattel, G. Wang, J. Mater. Chem. A 1 (2013) 10790–10797.
[31] G.W. Trucks, K. Raghavachari, G.S. Higashi, Y.J. Chabal, Phys. Rev. Lett. 65 (1990) 504–507.
[32] P.E. Blöchl, Phys. Rev. B 50 (1994) 17953.
[33] J.P. Perdew, K. Burke, M. Ernzerhof, Phys. Rev. Lett. 77 (1996) 3865.
[34] B. Barbiellini, E. Moroni, T. Jarlborg, J. Phys.: Condens. Matter 2 (1990) 7597.
[35] H.J. Monkhorst, J.D. Pack, Phys. Rev. B 13 (1976) 5188.
[36] F. Jaouen, S. Marcotte, J.-P. Dodelet, G. Lindbergh, J. Phys. Chem. B 107 (2003) 1376–1386.
[37] Y. Li, W. Zhou, H. Wang, L. Xie, Y. Liang, F. Wei, J.-C. Idrobo, S.J. Pennycook, H. Dai, Nat. Nanotechnol. 7 (2012) 394–400.
[38] N. Ramaswamy, S. Mukerjee, Adv. Phys. Chem. (2012) 17.
[39] H. Schulenburg, S. Stankov, V. Schünemann, J. Radnik, I. Dorbandt, S. Fiechter, P. Bogdanoff, H. Tributsch, J. Phys. Chem. B 107 (2003) 9034–9041.
[40] G. Liu, X. Li, P. Ganesan, B.N. Popov, Electrochim. Acta 55 (2010) 2853–2858.
[41] N. Ramaswamy, U. Tylus, Q. Jia, S. Mukerjee, J. Am. Chem. Soc. 135 (2013) 15443–15449.
[42] A.B. Anderson, Phys. Chem. Chem. Phys. 14 (2012) 1330–1338.
[43] F. Studt, Catal. Lett. 143 (2013) 58–60.
[44] C. Rovira, M. Parrinello, Int. J. Quantum Chem. 80 (2000) 1172–1180.
[45] E.F. Holby, C.D. Taylor, Sci. Rep. (2015) 5.
[46] M.S. Thorum, J.M. Hankett, A.A. Gewirth, J. Phys. Chem. Lett. 2 (2011) 295–298.
[47] J.H. Zagal, F. Bedioui, J.-P. Dodelet, N4-macrocyclic Metal Complexes, Springer Science & Business Media, 2007.
[48] U.I. Kramm, J. Herranz, N. Larouche, T.M. Arruda, M. Lefèvre, F. Jaouen, P. Bogdanoff, S. Fiechter, I. Abs-Wurmbach, S. Mukerjee, Phys. Chem. Chem. Phys. 14 (2012) 11673–11688.
[49] Q. Jia, N. Ramaswamy, H. Hafiz, U. Tylus, K. Strickland, G. Wu, B. Barbiellini, A. Bansil, E.F. Holby, P. Zelenay, S. Mukerjee, ACS Nano 9 (2015) 12496.
[50] S. Kattel, P. Atanassov, B. Kiefer, Phys. Chem. Chem. Phys. 15 (2013) 148–153.